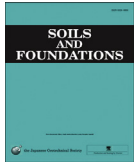# VICTORIA UNIVERSITY
MELBOURNE AUSTRALIA

A prediction model for the loading-wetting volumetric behavior of unsaturated granular materials

This is the Published version of the following publication

Technical Paper

A prediction model for the loading-wetting volumetric behavior of unsaturated granular materials ☆

Ehsan Yaghoubi [a,*], Mahdi M. Disfani [b], Arul Arulrajah [c], Asmaa Al-Taie [b]

[a] *College of Engineering and Science, Victoria University, Melbourne, Australia*
[b] *Department of Infrastructure Engineering, The University of Melbourne, Melbourne, Australia*
[c] *Department of Civil and Construction Engineering, Swinburne University of Technology, Melbourne, Australia*

Abstract

Geotechnical structures made of granular material tend to be unsaturated during their service life. However, there is presently a lack of sufficient research and studies on their volumetric behavior under unsaturated conditions. In this study, loading and wetting induced volumetric behavior of granular materials in the unsaturated state was studied within a moisture content-based framework. Recycled crushed brick (CB) and excavation waste rock (WR) were the granular materials used in this research to promote sustainable construction. Several loading, unloading, and wetting state paths were investigated with respect to virgin compaction surfaces (VCS) developed using groups of compaction curves. The obtained experimental data was utilized to develop a constitutive model capable of predicting wetting-induced volume changes of granular materials in a net stress range of 100–4000 kPa and gravimetric moisture content range of 3.6% for WR, and 7.5% for CB to saturation. The model was verified by undertaking several independent state paths on independent materials and comparing the experimental responses with those predicted using the model. The proposed model is featured with simplicity in acquiring the model input parameters with the aim of filling the existing gap between the theoretical and real-life application of unsaturated soil mechanics. An application of the model can be the basis for the prediction of the settlement of a granular geotechnical structure that is being externally loaded and is subject to changes in moisture content due to climatic effects.
© 2021 Production and hosting by Elsevier B.V. on behalf of The Japanese Geotechnical Society. This is an open access article under the CC BY-NC-ND license (http://creativecommons.org/licenses/by-nc-nd/4.0/).

Keywords: Loading-wetting path; Recycled materials; Unsaturated granular material; Volume change; Virgin compaction surface; MPK framework

1. Introduction

Unsaturated geomaterials are known to exhibit complicated behaviors, and the misinterpretation of their volumetric responses may cause damage to the infrastructures they support. In unsaturated geomechanics, it is well accepted that matric suction influences the behavior of soils similar to how the stress functions (Islam and Kodikara, 2015). Granular materials used in the construction of geotechnical structures, such as unbound pavement layers, structural fills or embankments are typically in an unsaturated state. However, fewer studies have been conducted to develop unsaturated constitutive models for unbound granular materials. This is partly due to relatively low magnitudes of suction in granular soils that do not justify the cost and complexities associated with specialized unsaturated testing procedures. The impact of suction is typically considered just for fine-grained soils, which exhibit significant suction values. In spite of that, Cary and Zapata (2011), Ba et al. (2013), Azam et al. (2013), and Yaghoubi et al. (2016) among others, demonstrated the importance of incorporating the unsaturated geomechanics

Nomenclature

e	void ratio
e_d	void ratio at the dry end
e_{d0}	void ratio at the dry end under p_{low}
e_{ini}^p	initial void ratios corresponding to e_{wini} under constant p
e_s	void ratio at saturation
e_{s0}	void ratio at saturation under p_{low}
e_w	moisture ratio (G_s ^{x} MC)
e_{wa}	average of e_{wm} and e_{ws}
e_{wd}	moisture ratio at the dry end
e_{wi}	moisture ratio of interest
e_{wini}	initial moisture ratio
e_{wm}	moisture ratio at MDD
e_{ws}	moisture ratio at saturation
$f(e_{wi})$	a function that gives Δe due to wetting from e_{wini} to e_{wi}
$g(e_{wi})$	a function that gives Δe due to wetting from e_{wd} to e_{wi}
G_s	specific gravity
LOO	line of optimum
MC	moisture content
MDD	maximum dry density

p	net stress ($=$total stress - u_a)
p_{low}	the lowest net stress used in the framework
p_L	the net stress at the end of loading
p_U	the net stress after unloading
S_r	degree of saturation
u_a	pore air pressure
u_w	pore water pressure
VCS	virgin compaction surface
α	hydric coefficient
Δe_{max}^p	maximum achievable Δe due to wetting from e_{wd} under the constant p
$(\Delta e_{max})_{ini}^p$	maximum achievable Δe due to wetting from e_{wini} under the constant p
Δe_{WT}	the change in void ratio due to wetting
Δe_U	the change in void ratio due to unloading
Δe_w	the change in moisture ratio
ζ	ratio of e_{wm}/e_{ws}
κ	unloading coefficient
λ_d	slope of compression line at e_{wd}
λ_s	slope of compression line at saturation
ψ	suction (u_a-u_w)

in interpreting the resilient behavior and permanent volume change characteristics of granular materials.

Constitutive models are frequently developed to predict the behavior of soils by proposing relationships between state variables through single-valued expressions (Fredlund and Rahardjo, 1993). The relationship between deformation state variables and stress state variables is expressed through volume change constitutive models. Traditionally, in unsaturated conditions, deformations due to loading and wetting are presented in the form of void ratio-net stress (e-p) and void ratio-suction (e-ψ) curves. Presentation of the constitutive models can be done through a constitutive (or state) surface within a 3D plot with two axes representing stress state variables and the third axis representing the deformation state variable.

The concept of unsaturated constitutive surfaces was first proposed by Matyas and Radhakrishna (1968), in which the developed surface related the void ratio and degree of saturation with matric suction and net stress. The state surface approach (SSA) incorporating suction was utilized by several researchers, and was significantly improved by Fredlund and Rahardjo (1993). However, since SSA models were based on an elastic analysis, they lacked the ability to fully explain the behavior of unsaturated soils that typically exhibit plastic behavior as well (Zhang and Li, 2011). As a result, researchers tended to prefer elasto-plastic models over SSA models. Alonso et al. (1990) proposed a comprehensive elasto-plastic model

capable of interpreting several aspects of unsaturated soils behavior. This model, termed as the Barcelona Basic Model (BBM), became the basis of several well-known future models, such as Cui and Delage (1996), Wheeler et al. (2003), and Vassallo et al. (2007). The BBM can be considered as the first elasto-plastic model that is mainly used to describe the volumetric response of unsaturated soils using suction as a constitutive parameter. The BBM framework developed a model and proposed a space to describe the isotropic stress states, being net mean stress and suction. In the BBM type models, a constitutive surface can be achieved using a group of loading-collapse curves, each corresponding to a constant suction. Each point at a loading-collapse contour on the surface represents a yield point obtained from suction-controlled oedometer testing. Using BBM type constitutive surfaces, if a sample is loaded to a certain yield stress under constant suction and then wetted to reach the suction equivalent to zero (saturation state), the sample would achieve maximum achievable collapse due to suction change. The minimum collapse is achieved if the sample is wetted under a constant stress equal or less than the yield stress corresponding to saturation state ($\psi = 0$).

BBM type models however have a few limitations (Zhang and Li, 2011). The first limitation in developing the loading-collapse and suction increase (drying) curves is an implicit, and arguably unrealistic, assumption that "identical" specimens have identical stress histories. The

next limitation is associated with the determination of model parameters. Even with the availability of suction controlled testing equipment and specialized testing staff, BBM type models use a limited number of test results with the aim of developing a model that is capable of interpreting soil behavior under any conditions. Another limitation with the BBM models is the uncertainty in the distinction between the elastic and plastic behavior of unsaturated soils. As a result, some researchers became willing to return to the constitutive surfaces and attempted to resolve the SSA limitations through development of a modified state surface approach (MSSA). An example of a successfully verified MSSA model was proposed by Zhang and Lytton (2009), and Zhang and Lytton (2012). In their modified state surface, Zhang and Lytton introduced a loading-unloading surface along the loading-collapse and suction increase curves to incorporate both elastic and plastic zones on the constitutive surface.

The development of a volume change model for unsaturated geomaterials requires applying at least one of the controlling state variables, being moisture content and suction (Gould et al., 2011). The state variable is defined as any "non-material variable required for characterizing a material system" (Fredlund and Rahardjo, 1993, Lu and Likos, 2004). Lu (2008) believes that any variable with the potential of substantial impact on the mechanical behavior can be taken as a stress state variable. As a result, both suction and moisture content could be considered as stress state variables. Although, accepting the moisture content as a state variable could be debatable, as moisture content does not incorporate stress units.

Some researchers have focused on developing moisture content (MC)-based frameworks, with the goal of developing a practical and cost-effective framework that worked with conventional testing methods, backed by a robust theoretical basis. Heath et al. (2004) developed a model to interpret the behavior of unsaturated granular materials that did not require the measurement of suction. Their model required void ratio, MC, and model parameters achievable through conventional triaxial tests. Kodikara (2012) proposed the most extensive MC-based framework being Monash-Peradeniya-Kodikara (MPK). In the MPK framework, a derivative of MC was incorporated in place of suction, based on the work input equation proposed by Houlsby (1997) in order to explain the volumetric behavior of compacted unsaturated fine soils. Kodikara (2012) incorporated "suction" indirectly, by stating that at a constant net stress, the soil water characteristic curve relates MC and suction. Experimental results of Gould et al. (2011) and Fleureau et al. (2002) show that in contrast to suction, in a condition that is environmentally stabilized, moisture ratio and void ratio do not exhibit hydraulic hysteresis. A similar conclusion can be drawn from experimental results presented by Raveendiraraj (2009) through comparing the hysteresis effect in void ratio-suction and void ratio-moisture ratio plots obtained from the behavior of kaolin. Kodikara (2012) concluded

that the significant void ratio-suction and moisture ratio-suction hysteresis may be minimized, if not eliminated, by coupling void ratio and moisture ratio. In the current research, the insignificant hysteresis between moisture content and void ratio was the rationale behind selecting a MC-based framework over conventional suction-based approaches. This was to meet an important objective of this research being the development of a prediction model with simplicity in achieving input parameters of the model through non-complex testing procedures available in typical geotechnical testing facilities.

The outcome of the MPK framework was a constitutive surface in the void ratio, moisture ratio (product of the specific gravity and MC) and net stress (e-e_w-p) space, formed by a number of compaction curves at various compaction pressures. The surface was named Loading-Wetting State Boundary Surface (LWSBS) and represented the loosest state of a compacted soil at any specific net stress and moisture ratio (Islam and Kodikara, 2015). Similar to BBM type constitutive surfaces, each point on LWSBS represents a yield point, therefore, if a sample at a certain e_w and e is loaded to a stress equivalent to the yield stress, then wetted to saturation, the maximum collapse would be achieved and the amount of the collapse could be predicted by following the e-e_w curve corresponding to the yield stress contour. The yield stress contour is in fact, the compaction curve of the yield (net) stress starting from (e, e_w) of interest to (e_{opt}, e_{wopt}), where e_{opt} and e_{wopt} represent void ratio and moisture ratio at optimum moisture content, respectively. Minimum collapse could be obtained if the same sample was loaded to a stress equal or less than the yield stress of the saturated sample.

The uniqueness of the LWSBS for unsaturated fine soils has been verified through several investigations including Islam and Kodikara (2015). Since its development, a few researchers have focused on expanding the application of the MPK framework application. Abeyrathne (2017) extended the application of the MPK framework to explain the deviatoric behavior of compacted clay, by developing a unique state surface in a space of specific volume, specific water volume (=1 + e_w) and net stress. Al-Taie et al. (2018) and Al-Taie et al. (2019) utilized the MPK framework in order to explain the collapse and swelling potential of lime treated highly expansive basaltic clay. They reported that a significant collapse and swelling potential existed when the lime-treated specimens were prepared at a high suction value and wetted under low net stresses even with specimens being stabilized with lime at optimum lime content. Kieu and Mahler (2018) incorporated suction in a LWSBS developed for a type of Hungarian high plasticity clay using the MPK framework and investigated the volumetric behavior of the soil with respect to changes in p, e_w, and ψ. They concluded that the MPK framework was able to explain not only the volumetric behavior of soils but also the shearing and tensile behavior of unsaturated soils. Jayasundara et al. (2019) advanced the MPK

framework by undertaking drying stress paths and verifying the uniqueness of the LWSBS during drying paths.

The MPK framework and the studies that have further verified or expanded the application of this framework have all been proven to be valid for fine-grained materials. However, the research work for expanding the application of the framework to unsaturated granular material is limited to Yaghoubi et al. (2019). The virgin compaction surface (VCS) developed by Yaghoubi et al. (2019) was partially capable of explaining the volumetric behavior of the granular material and was investigated through a limited number of the state paths and stress levels. Additional state paths through an extended experimental program was required for further investigation of the VCS which were carried out and presented in the current article.

In this paper, for the first time, a moisture content-based loading-wetting predictive model is presented and verified that is capable of providing an accurate interpretation of the volumetric behavior of unsaturated granular materials in a wide range of stress levels and moisture contents. Previous models of unsaturated granular materials may or may not give more accurate results compared to the current model; they, however, share a drawback from the geotechnical industry's perspective which is the need for specialized equipment for the determination of suction-based model parameters. For instance, Pham and Fredlund (2011) proposed a meticulous constitutive model, capable of predicting the volumetric responses of granular soils. Despite offering accurate volume change predictions and e-MC relationships, the model input parameters required unsaturated testing equipment, not readily available in many testing facilities.

The importance of a realistic interpretation of the loading-wetting volumetric response of granular material is clearly evident in climatic events. Precipitation or flooding can transform geotechnical structures, such as foundations of infrastructures, from a more stable unsaturated condition to a saturated condition. Understanding the volumetric response of granular geostructures to changes in the stress states caused by loading or wetting is crucial.

2. Background

Virgin compaction surfaces (VCS) for CB and WR were previously developed in a moisture content-based scheme using the experimental data obtained from a group of compaction curves (Yaghoubi et al., 2019). The VCS was developed by utilizing volume-mass relationship equations to convert the traditional compaction curves into e-e_w curves corresponding to net stresses of p (hereafter referred to as "stress contours"). Fig. 1 presents the VCS generated for CB in the (e-e_w-p) space in which the LOO represents the boundary between the dry and the wet sides of the developed surface. On the dry side, air can easily exit the soil, whereas on the wet side, the air could get trapped if the soil if loaded rapidly. Yaghoubi et al. (2019) proposed a predictive model for developing the VCS, as presented in Eqs. (1)–(4).
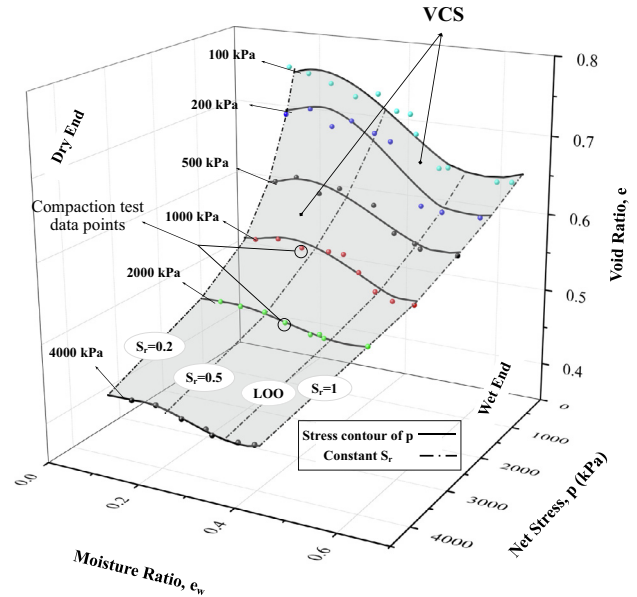

Fig. 1. The VCS developed for CB showing the stress contours in the space of e-e_w–p.

$$e = \left(\frac{e_d - e_s}{2}\right) \cos\left[\left(\frac{\pi}{e_{wa} - e_{wd}}\right)(e_w - e_{wd})\right]$$
$$+ \left(\frac{e_d + e_s}{2}\right) \tag{1}$$

$$e_s = e_{s0} - \lambda_s \ln\left(\frac{p}{p_{low}}\right) \tag{2}$$

$$e_d = e_{d0} - \lambda_d \ln\left(\frac{p}{p_{low}}\right) \tag{3}$$

$$e_{wa} = 0.5(1 + \zeta)e_s \tag{4}$$

Model parameters used in Eqs. (1)–(4) for developing the VCS of CB and WR are presented in Table 1 and defined in Notations.

Previously, a limited number of loading and wetting state paths were undertaken to investigate the applicability of developed VCSs, and the following outcomes were concluded:

- The VCSs were unique in incremental monotonic loading for the whole range of stress levels applied in the research (100–4000 kPa).

Table 1
Model parameters used for the development of VCS for CB and WR.

Model Parameter	CB	WR
e_{wd}	0.2	0.1
e_{s0}	0.65	0.682
e_{d0}	0.755	0.793
p_{low}	100 kPa	100 kPa
ζ	0.81	0.84
λ_s	0.065	0.069
λ_d	0.091	0.087

- The uniqueness of the VCSs with respect to wetting was only verified for stress levels greater than 2000 kPa.

In the abovementioned model, the loading and wetting induced volumetric behavior of the material was not fully addressed. Also, the unloading state paths were not investigated with respect to VCS. In this paper, the focus was placed on undertaking more loading and wetting state paths in order to further evaluate the uniqueness of developed surfaces, as well as investigating unloading state paths, and the ultimate goal was to develop a more accurate constitutive model for interpreting the volumetric behavior of the unsaturated granular material in a wider range of stress levels compared to the previous model.

3. Experimental program

3.1. Materials

The recycled granular materials used in this research were Crushed Brick (CB), and Waste Rock (WR) sourced from recycling industries in the state of Victoria, Australia. The reuse of waste granular materials was aimed to promote sustainable design and construction. Table 2 presents the geotechnical properties of CB and WR that were used for the development of the model proposed in this research. In preparation of the granular samples for the state path tests, as a measure to achieve maximum consistency, two control sieves were used to split the materials into three portions as presented in Fig. 2. These three portions were mixed in specific percentages, achieved from the particle size distribution (PSD) of the as-received material.

The tactile assessment, together with scanning electron micrographs presented in Fig. 3 (2000 times magnified) indicate that CB particles (Fig. 3(a)) have a rougher surface compared to WR particles (Fig. 3(b)) and hence, greater internal friction. Fig. 3 also shows the presence of micropores in the CB particle, which could result in CB samples having dual porosity. However, reviewing soil water characteristics curves (SWCC) of CB blends available in the literature (Azam et al. (2013) and Azam et al. (2014) among others) does not show similarities with SWCC of the granular material with dual porosity. A CB sample compacted to the modified Proctor MDD at moisture content of 7.5% (the driest state of CB in this research) will have a range of

suction between 1 and 5 kPa estimated using Aubertin et al. (2003) and Perera et al. (2005) predictive models. This range for WR at the driest state of WR in this research (3.6%) is 0.7 to 1.5 kPa. CB and WR have estimated suction of less than 1 kPa and 0.5 kPa at close-to-saturation states, respectively.

3.2. Testing equipment

The testing equipment consisted of a loading system, the testing mold, and accessories. The loading system was a UTM-100 machine (100 kN capacity) equipped with a load cell and Linear Variable Differential Transformer (LVDT) connected to a data logger in order to record the stress and deformations during the tests. Three openings in the wall of the mold and three openings on the loading plate allowed for the controlled injection of water (wetting) from the top and sides of the sample during the tests. The testing equipment are presented in Fig. 4. During the tests, drainage was allowed from the top of the sample. Lubricating grease was used on the internal wall of the mold to reduce the influence of friction between soil and mold.

3.3. Loading, unloading and wetting procedures

The state paths conducted in this research included Loading-Wetting (LW), Loading-Unloading–Wetting (LUW) and Loading-Wetting-(greater) Loading-Wetting
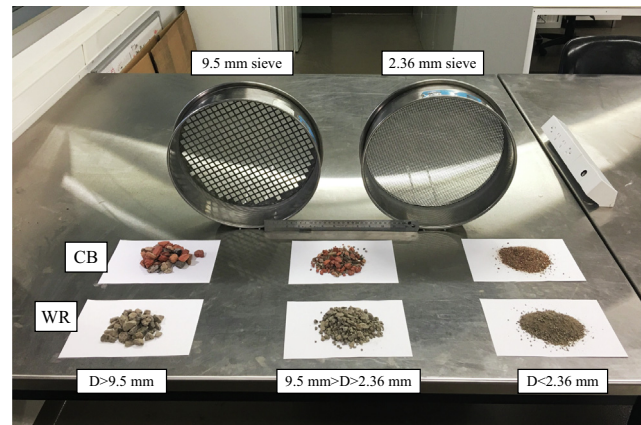

Fig. 2. CB and WR samples split into three portions for sample reconstitution.

Table 2
Geotechnical properties of CB and WR.

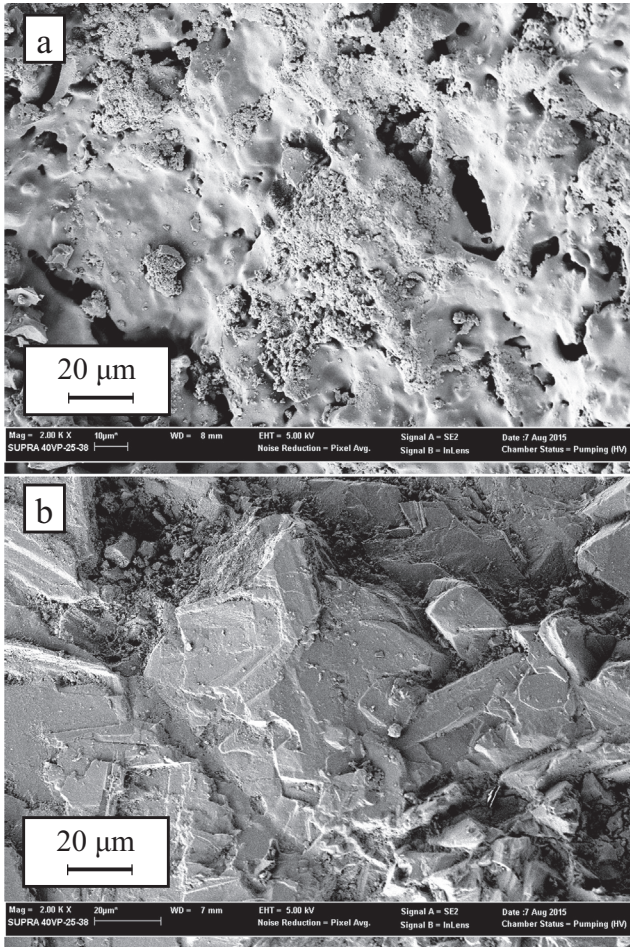| Material	Specific gravity, Gs	Fine content (%) [particles finer than 0.075 mm]	Maximum particle size (mm)	Maximum Dry Density (kg/m3)	Optimum moisture content (%)	Water absorption (%)	Hydraulic conductivity (m/s)
Crushed Brick (CB)	2.64	6	19	1990	10.8	6.6	1.16×10^{-6}
Waste Rock (WR)	2.82	4	19	2220	5.7	4.1	2.45×10^{-6}

Fig. 3. Scanning Electron Micrographs of (a) a CB particle, and (b) a WR particle.

(LWLW). An example of each of these state paths is indicated in Fig. 5, in which point O is the starting point. Depending on the MC of the sample, in order to prevent the possible build-up of pore water pressure, two different loading rates were applied until the target net stress (p) was achieved. Loading rates of approximately 500 kPa/min and 50 kPa/min were applied to samples with MCs lower or higher than their modified Proctor optimum moisture contents (OMC), respectively, as presented in Table 2. An unloading rate of approximately −500 kPa/min was used for all samples. On reaching the target p, static pressure was kept constant on the sample until no further deformation was observed.

Controlled wetting was achieved through the injection of a predetermined amount of water using a graded syringe. The calculated amount of water corresponding to a 2% increase in the moisture content was added at reaching a constant displacement reading in the current moisture content. Following each injection, the openings were covered with cellophane sheets to prevent evaporation. Increment of moisture content was carried out in steps until the saturation state was achieved. In this experimental program, drying paths were not carried out, as the focus of the

research was on the settlement of a granular geostructure due to wetting. In any case, unlike fine-grained soils, such as clay, granular materials, especially those in a compacted state are not known to exhibit shrink (or swell) behavior as a result of drying. As an example, base/subbase layers compacted at their optimum moisture content may commence drying after compaction; however, they are not expected to settle due to moisture loss. Fig. 6 shows the recorded deformation due to loading, as well as wetting, during a LWLW state path in a deformation-time plot.

4. Developed VCS and the state paths

Two conditions need to be met in order to verify the uniqueness of the developed VCS. First, whether the state paths travel along their corresponding contour of constant net stress or constant moisture ratio on the developed VCS. For instance, by loading the sample with the moisture ratio of e_w to the net stress of p, the state path reaches the VCS at the point corresponding to p and e_w. Second, whether the surface is path-independent. Verification of the path-independence can be achieved through a series of independent state paths on identical samples, whereby a state path describes the changes in the state of the soil (Fredlund and Rahardjo, 1993).

4.1. Loading-wetting paths

The LW state paths conducted on CB and WR samples are listed in Tables 3 and 4, respectively. In these tables, the value in parentheses after L refers to the net stress (p) and "sat" refers to the saturation condition. Additional LW paths compared to limited paths in Yaghoubi et al. (2019) were carried out to cover a variety of net stresses and initial moisture ratios. Four LW paths conducted on CB and WR are selected to be presented in Fig. 7 and due to similar behavior of CB and WR, for brevity, the response on CB is discussed in this section.

Fig. 7(a) shows two state paths for CB, being CB-L(100)W(sat)-2 and CB-L(4000)W(sat)-1 in Table 3, and the VCS developed for CB in the space of e-e_w-p. In CB-L(100)W(sat)-2 path (dashed line), loading the sample from a loose state to p = 100 kPa at e_w = 0.35 resulted in reaching the stress contour of 100 kPa on the VCS (point A). However, by wetting the sample under constant p of 100 kPa, the state path and the stress contour diverge. Similar behavior was observed by conducting the LW paths under net stresses of up to and including 1000 kPa presented in Table 3. This showed that at stress levels less than 2000 kPa, the loading state path was predictable using the VCS, whereas the wetting path was not. In CB-L(4000)W(sat)-1 path a stress level of 4000 kPa was targeted. The sample was loaded from a loose state at e_w = 0.2 to p = 4000 kPa (point A'), and from there was wetted to saturation under constant p of 4000 kPa (point B'). Fig. 7(a) indicates that the loading path, at constant e_w = 0.2, follows the VCS and reaches the stress contour of 4000 kPa at point A'. This
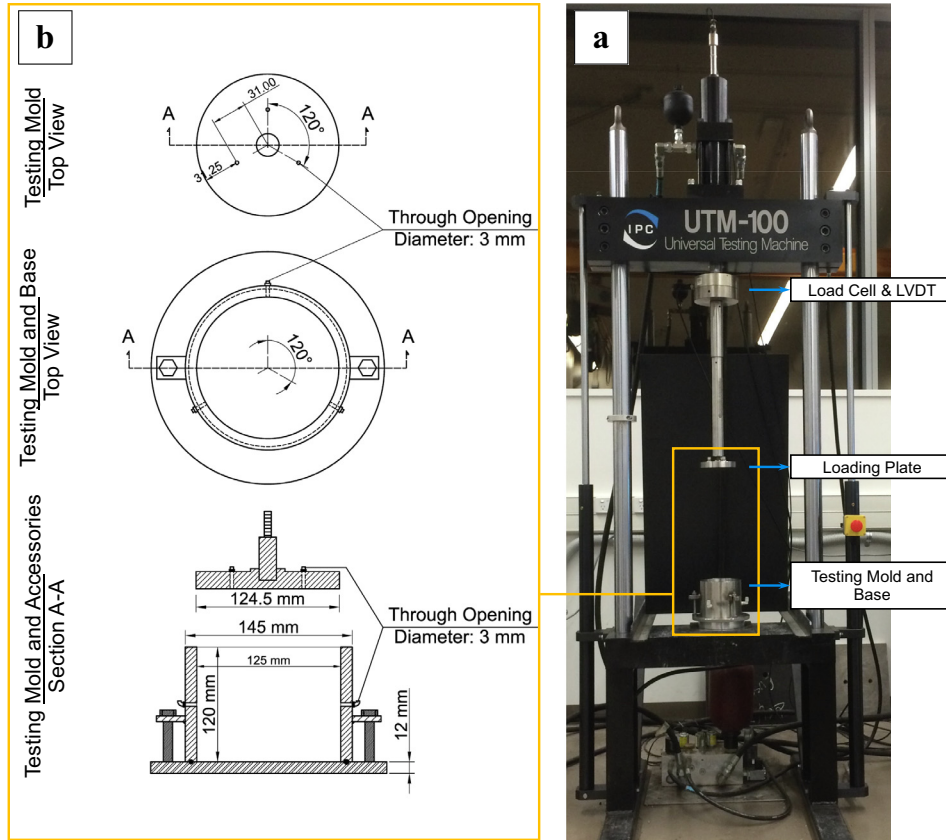
Fig. 4. Testing equipment: (a) image of the compaction mold, loading frame and the accessories, (b) detailed drawings of the mold, base and loading plate.

was expected since the VCS is defined as the loosest state of the sample at any specific p and e_w of interest. Interestingly, the wetting path followed the stress contour of 4000 kPa. Similar behavior was observed when specimens were prepared at different moisture ratios and loaded to the stresses of 2000 kPa and 4000 kPa and then wetted to saturation. This showed that both loading and wetting-induced deformations were predictable using the VCS, provided that the wetting path was undertaken under stress levels greater than 2000 kPa. Undertaking several more LW paths on WR samples, such as those presented in Fig. 7(b) with different initial e_w and p, further supported the conclusions made based on LW paths on CB.

The state paths listed in Tables 3 and 4, also indicated that the deformation through wetting was to a great extent lower when the initial e_w was shifted towards the wet end on the surface. This can be explained by the typical SWCC shape for granular materials, although the focus of the current research is working within a moisture content-based framework. Changes in moisture content close to the dry end of the SWCC result in greater changes in suction compared to those resulted by the same moisture variation closer to the wet end of the SWCC. For instance, while the change of Sr from 80% to 90% results in 0.06 kPa reduction of suction for WR, following Perera et al. (2005) prediction, increasing Sr from 10% to 20% results in 9.7 kPa reduction of suction, which is about 160 times greater. A

greater change in suction, as an internal stress, due to the change in MC allows for greater deformation compared to a lower suction change caused by the same change in MC.

4.2. Loading-unloading-wetting paths

The LUW state paths conducted on CB and WR are listed in Table 5. In Table 5, the value in parentheses after L and U refers to the net stress (p) and "sat" refers to the saturation condition. The paths were selected to cover several net stresses and difference between stress levels, as well as several initial moisture ratios. Two of the LUW paths were selected to be presented and discussed in this section (Fig. 8).

Fig. 8(a) shows CB-L(1000)U(500)W(sat) path and the VCS developed for CB. In this figure, the sample was loaded from a loose state (point O) at $e_w = 0.23$ to p = 1000 kPa (point A), unloaded to p = 500 kPa (point B) at the same e_w, and finally wetted to saturation under p = 500 kPa (point C). The loading path (OA) reached the stress contour of 1000 kPa while closely following the e_w contour of 0.23. By unloading the sample, the state path moved away from the VCS to the space under the surface. This was due to the fact that VCS represents the loosest state of the sample at any p and e_w while the sample at point B had experienced a net stress greater than
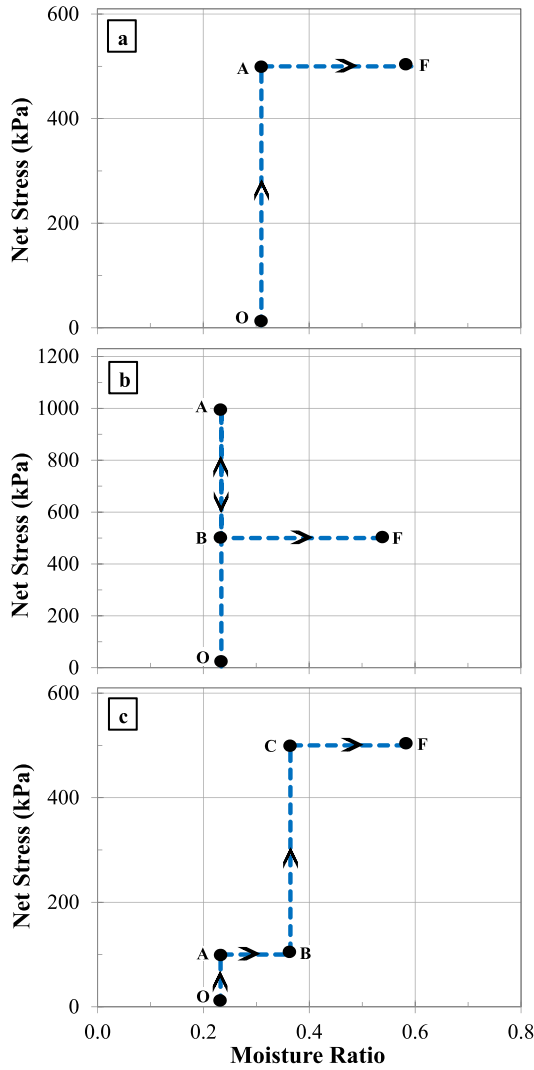
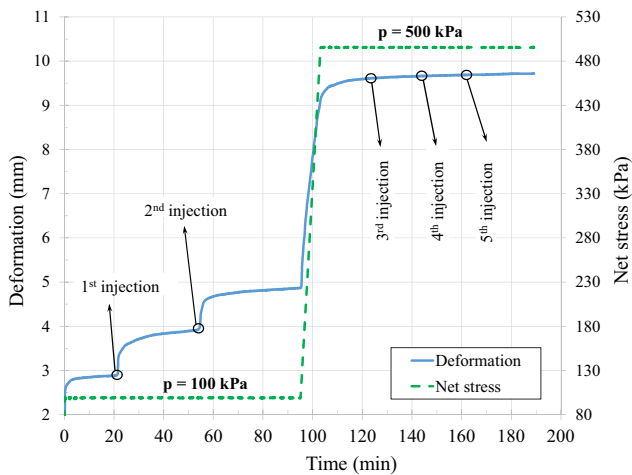Fig. 5. An example of state paths of (a) LW, (b) LUW, and (c) LWLW.

Fig. 6. An example of deformation-time plot during a LWLW state path.

500 kPa, i.e. 1000 kPa at point A. By wetting the sample under p = 500 kPa, the state path moved towards the

$S_r = 1$ line. However, the path did not reach the stress contour corresponding to p = 500 kPa. Therefore, the state path remained under the surface from its driest to its wettest condition. A similar pattern was observed in other LUW paths carried out on CB samples listed in Table 5.

Fig. 8(b) demonstrates the WR-L(4000)U(100)W(sat) path and the VCS developed for WR. In this path, the WR sample was loaded from a loose state at $e_w = 0.14$ to p = 4000 kPa (point A), unloaded to p = 100 kPa (point B), and finally wetted to saturation under p = 100 kPa (point C). By unloading the sample to a lower stress level, the state path moved to the space under the VCS. By wetting the unloaded sample to the saturation condition under p = 100 kPa, the state path did not reach the stress contour of 100 kPa, as it had experienced a significantly denser state under p = 4000 kPa. Experimental results of LUW paths listed in Table 5 revealed the uniqueness of the VCS with respect to loading. However, wetting the sample under a constant stress that was lower that the compaction stress could not be interpreted using the developed VCS.

LUW paths presented in Table 5 were further investigated by calculating the unloading coefficient (κ) and hydric coefficient (α) obtained from the LUW state paths. The unloading coefficient is the gradient of changes in e due to unloading at a constant e_w. The hydric coefficient is the gradient of changes in the e due to changes in e_w under constant p. Coefficients of κ and α for each e_w or p were calculated using Eqs. (5) and (6) and presented in Table 6.

$$\alpha = \frac{\Delta e_{WT}}{\Delta e_w} \tag{5}$$

$$\kappa = \frac{\Delta e_U}{ln \frac{p_U}{p_L}} \tag{6}$$

where Δe_{WT} is the change in void ratio due to wetting from the initial e_w to the final e_w (B-C paths in Fig. 8), Δe_U is the change in void ratio due to unloading, Δe_w is the change in moisture ratio, p_L is the net stress at the end of loading, and p_U is the net stress after unloading.

It is revealed that the values of Δe_{WT} are close to zero. In other words, samples that had undergone a higher load of p_L do not show a considerable volume change through wetting under a lower load of p_U. The results in Table 6 also indicate that α coefficients are generally lower than κ coefficients and both α and κ are very close to zero. A hydric coefficient (α) of 0.222 was reported for kaolin sample loaded to $p_L = 1000$-kPa, unloaded to $p_U = 500$ kPa and wetted under the same p_U in Islam (2015). Under the same stress levels of loading–unloading, a significantly lower α coefficient of 0.002 was obtained for CB (and correspondingly for WR).

In LUW paths presented by Islam and Kodikara (2015), the kaolin sample unloaded to the net stress of p initially expanded during wetting until reaching the VCS and from there followed the surface. In other words, the void ratio of the unloaded sample initially increased through wetting. This could be due to the reduction of inter-particle suction pressure during wetting. In compacted samples of CB and

Table 3
A summary of the LW state paths carried out on CB.

Path ID	Initial e_w	Test Description
CB-L(100)W(sat)-1	0.20	Loading from a loose state at MC = 7.6% to p = 100 kPa and wetting under p = 100 kPa to saturation
CB-L(100)W(sat)-2	0.35	Loading from a loose state at MC = 13.4% to p = 100 kPa and wetting under p = 100 kPa to saturation
CB-L(200)W(sat)	0.34	Loading from a loose state at MC = 12.7% to p = 200 kPa and wetting under p = 200 kPa to saturation
CB-L(500)W(sat)-1	0.20	Loading from a loose state at MC = 7.6% to p = 500 kPa and wetting under p = 500 kPa to saturation
CB-L(500)W(sat)-2	0.31	Loading from a loose state at MC = 11.7% to p = 500 kPa and wetting under p = 500 kPa to saturation
CB-L(1000)W(sat)-1	0.20	Loading from a loose state at MC = 7.6% to p = 1000 kPa and wetting under p = 1000 kPa to saturation
CB-L(1000)W(sat)-2	0.27	Loading from a loose state at MC = 10.2% to p = 1000 kPa and wetting under p = 1000 kPa to saturation
CB-L(2000)W(sat)	0.25	Loading from a loose state at MC = 9.5% to p = 2000 kPa and wetting under p = 2000 kPa to saturation
CB-L(4000)W(sat)-1	0.20	Loading from a loose state at MC = 7.6% to p = 4000 kPa and wetting under p = 4000 kPa to saturation
CB-L(4000)W(sat)-2	0.23	Loading from a loose state at MC = 8.7% to p = 4000 kPa and wetting under p = 4000 kPa to saturation

Table 4
A summary of the LW state paths carried out on WR.

| Path ID	Initial e_w	Test Description
WR-L(100)W(sat)-1	0.10	Loading from a loose state at MC = 3.6% to p = 100 kPa and wetting under p = 100 kPa to saturation
WR-L(100)W(sat)-2	0.13	Loading from a loose state at MC = 4.5% to p = 100 kPa and wetting under p = 100 kPa to saturation
WR-L(100)W(sat)-3	0.17	Loading from a loose state at MC = 6% to p = 100 kPa and wetting under p = 100 kPa to saturation
WR-L(200)W(sat)	0.17	Loading from a loose state at MC = 6.1% to p = 200 kPa and wetting under p = 200 kPa to saturation
WR-L(500)W(sat)-1	0.10	Loading from a loose state at MC = 3.6% to p = 500 kPa and wetting under p = 500 kPa to saturation
WR-L(500)W(sat)-2	0.14	Loading from a loose state at MC = 5% to p = 500 kPa and wetting under p = 500 kPa to saturation
WR-L(500)W(sat)-3	0.17	Loading from a loose state at MC = 6% to p = 500 kPa and wetting under p = 500 kPa to saturation
WR-L(1000)W(sat)-1	0.10	Loading from a loose state at MC = 3.6% to p = 1000 kPa and wetting under p = 1000 kPa to saturation
WR-L(1000)W(sat)-2	0.14	Loading from a loose state at MC = 5% to p = 1000 kPa and wetting under p = 1000 kPa to saturation
WR-L(2000)W(sat)	0.17	Loading from a loose state at MC = 6.1% to p = 2000 kPa and wetting under p = 2000 kPa to saturation
WR-L(4000)W(sat)-1	0.10	Loading from a loose state at MC = 3.8% to p = 4000 kPa and wetting under p = 4000 kPa to saturation
WR-L(4000)W(sat)-2	0.17	Loading from a loose state at MC = 6.1% to p = 4000 kPa and wetting under p = 4000 kPa to saturation
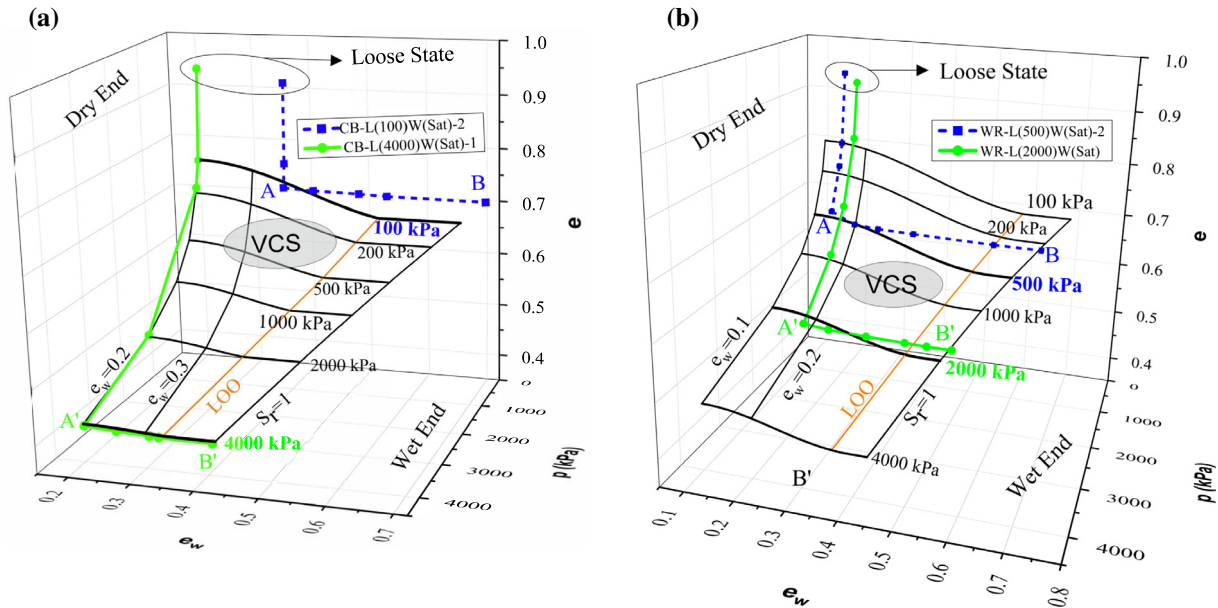
Fig. 7. The state paths of (a) CB-L(100)W(sat)-2 and CB-L(4000)W(sat)-1, and (b) WR-L(500)W(sat)-2 and WR-L(2000)W(sat), and their corresponding VCS, in the space of e-e_w-p.

WR, changes in suction before and after wetting was limited to a maximum of 10 kPa (Yaghoubi et al., 2017). Thus, unlike the non-swelling kaolin sample, the reduction of suction did not have a significant influence on the volume change of the compacted sample. The interlock due to internal friction between the relatively rough CB and WR particles prevented the sample from expansion due to wetting. Hence, the hydric coefficient was close to zero.

Table 5
A summary of the LUW state paths carried out on CB and WR.

Path ID	Initial e_w	Test Description
CB-L(500)U(100)W(sat)	0.20	Loading CB sample from a loose state at MC = 7.7% to p = 500 kPa, unloading to p = 100 kPa wetting under p = 100 kPa to saturation
CB-L(1000)U(500)W(sat)	0.23	Loading CB sample from a loose state at MC = 8.9% to p = 1000 kPa, unloading to p = 500 kPa wetting under p = 500 kPa to saturation
CB-L(4000)U(100)W(sat)	0.27	Loading CB sample from a loose state at MC = 10.1% to p = 4000 kPa, unloading to p = 100 kPa wetting under p = 100 kPa to saturation
WR-L(200)U(100)W(sat)	0.12	Loading WR sample from a loose state at MC = 4.1% to p = 200 kPa, unloading to p = 100 kPa wetting under p = 100 kPa to saturation
WR-L(500)U(200)W(sat)	0.10	Loading WR sample from a loose state at MC = 3.6% to p = 500 kPa, unloading to p = 200 kPa wetting under p = 200 kPa to saturation
WR-L(4000)U(100)W(sat)	0.14	Loading WR sample from a loose state at MC = 5% to p = 4000 kPa, unloading to p = 100 kPa wetting under p = 100 kPa to saturation
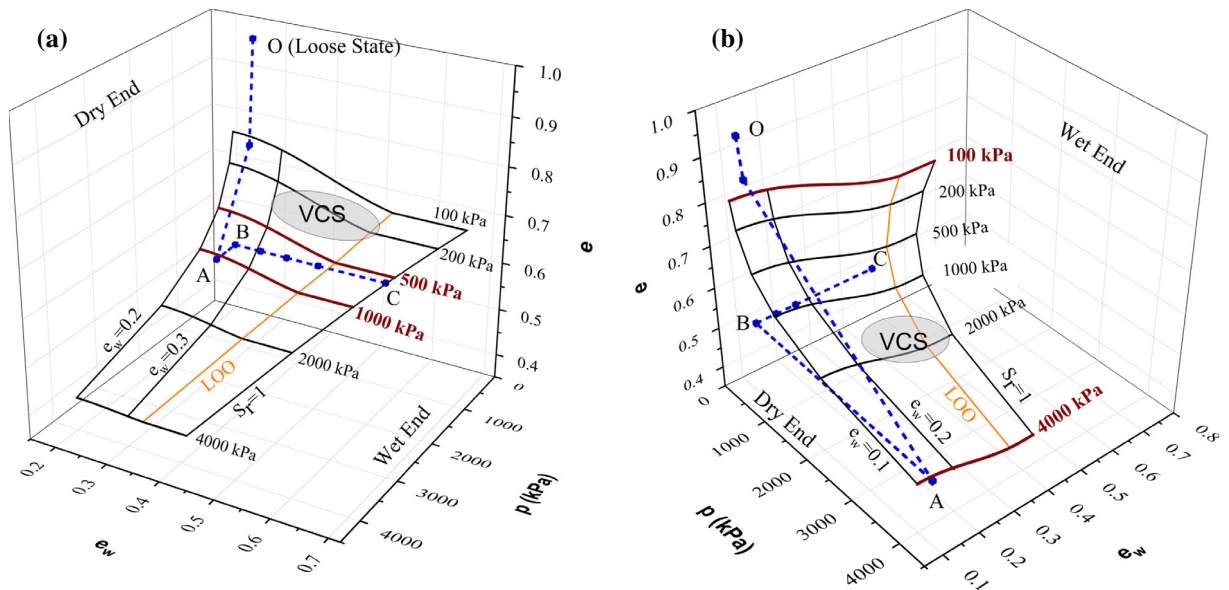
Fig. 8. The state paths of (a) CB-L(1000)U(500)W(sat), and (b) WR-L(4000)U(100)W(sat), and their corresponding VCS, in the space of e-e_w-p.

4.3. Loading-wetting-loading-wetting paths

The LWLW state paths are a combination of two LW paths starting from two different moisture ratios. The LWLW state paths conducted on CB and WR samples are listed in Table 7. The LWLW paths were selected in order to cover different stress levels, as well as several initial moisture ratios. Two of the LWLW paths were selected to be presented in Fig. 9 and due to similar behavior of CB and WR, for brevity, the response on CB samples is discussed in this section.

Fig. 9(a) shows the CB-L(100)W(0.36)L(500)W(sat) path and the VCS developed for CB. In this path, the CB sample was loaded from a loose state (point O) at $e_w = 0.23$ to p = 100 kPa (point A), wetted to $e_w = 0.36$ (point B), then loaded to p = 500 kPa (point C), and finally wetted to saturation under p = 500 kPa (point D). The loading paths (OA and BC) reached their corresponding stress contours. Wetting paths (AB and CD), however, did not closely follow their corresponding stress contours.

This is in agreement with the conclusion made before, based on the LW paths that the wetting path under low stress levels, such as 200 kPa and 500 kPa cannot be interpreted accurately by the VCS.

As demonstrated in Fig. 9(b) both loading paths of OA and BC reached their corresponding stress contours on the VCS of WR. While the wetting path of CD closely followed, although not as closely as CB samples, the corresponding e-e_w curve for p = 4000 kPa, the curve for p = 100 kPa was not followed by the AB path. This further verified the previously made conclusion that the wetting paths follow the VCS provided that the stress level is greater than 2000 kPa. In Fig. 9, BC paths only indicate the beginning and end-point of the loading path and no data were collected between A and B.

4.4. Discussion on the uniqueness of the developed VCS

Conducting several LW state paths with initial moisture contents ranging from 3.9% to 13.4% under constant net

Table 6
Unloading and hydric coefficients of CB and WR.

Path ID	Δe_w	Δe_{WT}	Δe_U	α	κ
CB-L(500)U(100)W(sat)	0.294	0.0001	0.004	0.000	−0.002
CB-L(1000)U(500)W(sat)	0.169	−0.0003	0.003	−0.002	−0.004
CB-L(4000)U(100)W(sat)	0.068	0.0002	0.023	0.003	−0.006
WR-L(200)U(100)W(sat)	0.421	−0.0002	0.001	−0.001	−0.002
WR-L(500)U(200)W(sat)	0.405	0.0000	0.002	0.000	−0.003
WR-L(4000)U(100)W(sat)	0.209	0.0003	0.024	0.001	−0.006

Table 7
A summary of the LWLW state paths carried out on CB and WR.

Path ID	Initial e_w	Test Description
CB-L(200)W(0.28)L(4000)W(sat)	0.20	Loading CB sample from a loose state at MC = 7.6% to p = 200 kPa, wetting to MC = 10.6% under p = 200 kPa, then loading to p = 4000 kPa and wetting under p = 4000 kPa to saturation
CB-L(100)W(0.36)L(500)W(sat)	0.23	Loading CB sample from a loose state at MC = 8.8% to p = 100 kPa, wetting to MC = 13.8% under p = 100 kPa, then loading to p = 500 kPa and wetting under p = 500 kPa to saturation
CB-L(500)W(0.31)L(1000)W(sat)	0.20	Loading CB sample from a loose state at MC = 7.7% to p = 500 kPa, wetting to MC = 11.7% under p = 500 kPa, then loading to p = 1000 kPa and wetting under p = 1000 kPa to saturation
WR-L(100)W(0.22)L(4000)W(sat)	0.13	Loading WR sample from a loose state at MC = 4.7% to p = 100 kPa, wetting to MC = 7.7% under p = 100 kPa, then loading to p = 4000 kPa and wetting under p = 4000 kPa to saturation
WR-L(100)W(0.26)L(500)W(sat)	0.12	Loading WR sample from a loose state at MC = 4.3% to p = 100 kPa, wetting to MC = 9.3% under p = 100 kPa, then loading to p = 500 kPa and wetting under p = 500 kPa to saturation
WR-L(500)W(0.22)L(1000)W(sat)	0.10	Loading WR sample from a loose state at MC = 3.7% to p = 500 kPa, wetting to MC = 7.7% under p = 500 kPa, then loading to p = 1000 kPa and wetting under p = 1000 kPa to saturation

stresses of 100–4000 kPa showed that the developed VCSs were unique with respect to loading. However, in wetting paths, the surface was only unique under net stresses higher than 2000 kPa. Comparison of the measured and predicted void ratios during wetting paths under stress levels greater than 2000 kPa, following Witczak et al. (2002) criteria showed "Excellent" and "Good" accuracy. The accuracy of the predicted data is presented in Table 8. In this table, R^2 is the coefficient of determination, S_e is the standard error of estimate and S_y is the standard deviation. Evidently, the predicted response of CB samples showed a better correlation with the experimental data compared to that of WR. Also, the LWLW state paths carried out for several stress levels and initial moisture ratios were in agreement with the results of individual LW state paths.

The path-independence of the developed VCS was previously verified by Yaghoubi et al. (2019). They showed that for CB and WR, both Loading-Wetting (LW) and
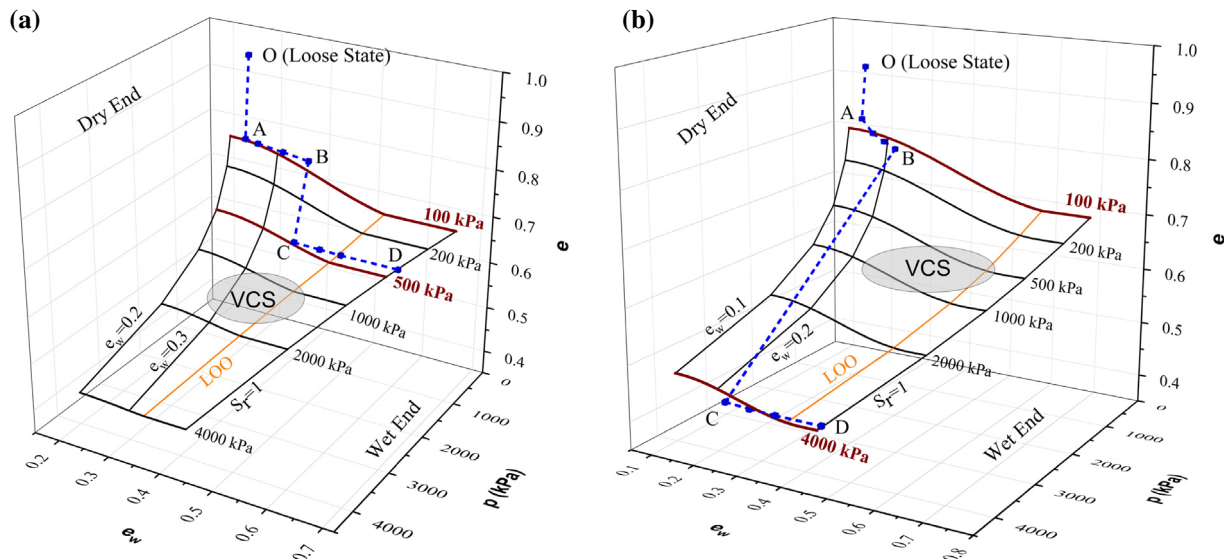

Fig. 9. The state paths of (a) CB-L(100)W(0.36)L(500)W(sat) and (b) WR-L(100)W(0.22)L(4000)W(sat), and their corresponding VCS, in the space of e-e_w-p.

Table 8
Evaluation of the accuracy of predicted data.

Material	State Path	No. of data points (n)	R^2	Se/Sy	Witczak et al. (2002) criteria
CB	Wetting under p ≥ 2000 kPa	13	0.97	0.19	Excellent
WR	Wetting under p ≥ 2000 kPa	16	0.72	0.53	Good

Wetting-Loading (WL) state paths with the same initial and final moisture and net stress conditions reached a close location on their corresponding VCS, provided that the final net stress level was equal or greater than 2000 kPa.

The LUW state paths revealed three points. Firstly, the uniqueness of the surface with respect to loading was further verified. In all the LUW paths, loading a sample to the net stress of p, took the path to the corresponding stress contour on the VCS. Secondly, when the sample was unloaded to a lower net stress, the path was directed from the surface to underneath the surface, confirming that the VCS is a set of all points that represent the loosest state at a given net stress and void ratio. Thirdly, if the sample unloaded to the net stress of p and wetted under constant p until it intercepted the stress contour of p, the surface would not have been followed afterwards (e.g. Fig. 8). This showed that the uniqueness of the surface due to changes in the state variable of net stress was limited to monotonic loading. In other words, the VCS is only followed in incremental monotonic loading (increasing p), and monotonic wetting (increasing e_w).

4.5. Limitations of the developed VCS

The developed VCSs are applicable to stress levels between 100 kPa and 4000 kPa. Therefore, the initial loading paths from a loose state to sample compacted to 100 kPa cannot be interpreted using the surface. The selection of the lower limit, i.e. 100 kPa, was through a basic estimation of the vertical stress at a depth of 250 mm caused by a vehicle with approximately 500 kPa pressure at the pavement-tire interface, using Foster and Ahlvin (1954) chart for the distribution of vertical stress due to circular area loading. The selection of the upper limit, i.e. 4000 kPa was due to the capacity of the testing tools and equipment.

The proposed VCSs that generate a direct relationship between the traditional compaction curves and the constitutive deformation response of soils aim to provide a simple approach for practical engineering applications as explained in Section 7 of this article. However, even though partially, as discussed in Sections 4.1–4.3, VCSs cannot fully illustrate the complex behavior of unsaturated granular materials such as loading-unloading-reloading and wetting-drying paths.

Advocating the use of moisture ratio does not undermine the work that can be done on hysteresis with suction. The lack of directly incorporating suction in the moisture content-based framework is not theoretically incorrect; rather, it makes this approach a partial theory with the goal of developing a method in which some difficulties and complexities with previous models can be resolved. Incorporating suction is required as a state variable in the water flow equation. Nevertheless, moisture diffusivity can also be used to model the water flow and hence, the equation can be developed using moisture content alone (Al-Taie et al., 2019). Although, this approach is limited to modelling a single material layered system. In two or more layered systems, the suction in the interface between the two materials is the same, but the moisture contents of the two materials can be different, and hence, the SWCC is needed to relate the suction to the corresponding moisture contents.

4.6. The need for an accurate model to predict the volume changes

The wetting part of the LW paths presented in Tables 3 and 4 showed relatively smaller volume changes compared to those of fine materials, especially when the sample was under higher net stresses. In granular geostructures such as unbound pavement base and subbase courses which are normally well compacted and contain low fine contents, relatively small volume changes occur through wetting (Heath et al., 2004). Based on the estimation of suction values using Aubertin et al. (2003) and Perera et al. (2005) models, reduction of suction ($\Delta\psi$) for CB wetted from $S_r = 0.48$ to $S_r = 1$ under p ≈ 200kpa was less than 2 kPa (1% of p) and 10 kPa (5% of p), respectively. In the same wetting and loading regime, $\Delta\psi$ of approximately 150 kPa (75% of p) for pearl clay in Sun et al. (2007) and 500 kPa (250% p) in Islam (2015) for kaolin was achieved.

In spite of low volume changes of the compacted granular material through wetting, accumulation of small volume changes eventually results in major distresses such as rutting. The investigation of the state paths, revealed that the VCS is incapable of accurately predicting the wetting induced deformations under net stresses lower than 2000 kPa. Granular materials are known to show notably different volumetric behavior under low net stresses compared to higher pressure conditions (Macari-Pasqualino et al., 1994). High internal frictions between rough-surfaced particles of granular materials and low suction pressure in these materials could result in a different response in LW state paths, leading to the wetting paths not following the developed VCS in low stress levels. In the case of WR, even at stress levels greater than 2000 kPa, the accuracy of the predicted paths was "Good" and not "Excellent". These observations necessitate the development and validation of a more accurate model to

interpret the volumetric behavior of the loaded samples during the wetting state paths.

5. Development of the wetting path model

In order to develop the wetting path model, the e-e_w curves of the wetting part of the LW paths were carefully observed. The wetting paths under any specific constant net stress, starting from different void ratios depending on their initial moisture condition, generally formed nearly parallel curves, based on observing experimental results of 22 LW paths (a total of 53 and 84 data points for CB and WR, respectively). More experimental results could further verify this conclusion. Fig. 10, shows two wetting curves under the constant p of 500 kPa for WR, as an example. The wetting path of the continuous curve started at initial moisture ratio (e_{wini}) of 0.1 and the path of the dashed curve started from a greater e_{wini} of 0.14. Even though, the values of initial void ratios corresponding to e_{wini} under constant net stress of p (e_{ini}^p) were not the same, both curves followed a nearly parallel trend. The curves tended to change to a linear shape as the sample became wetter than the moisture ratio of 0.2. The same behavior was observed in all wetting paths presented in Tables 3 and 4. This indicated that the void ratio of interest under the net stress of p (e_i^p) corresponding to a moisture ratio of interest (e_{wi}) could be achieved using Eq. (7).

$$e_i^p = e_{ini}^p - f(e_{wi}) \tag{7}$$

where $f(e_{wi})$ is a function of e_w that gives the reduction of e due to wetting from e_{wini} to e_{wi}.

Two sets of information were required for predicting the volume change due to wetting. First, a wetting path from the driest point of interest (e_{wd}) to saturation, which was achievable by conducting a single wetting state path test. This gave the maximum achievable reduction of void ratio due to wetting under the constant net stress of p (Δe_{max}^p). Second, the state where the wetting started (e_{wini}, e_{ini}^p). Value of e_{ini}^p could be achieved from Eq. (1).
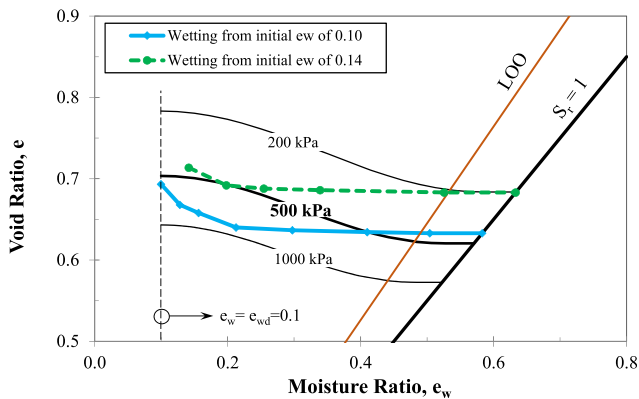

Fig. 10. Close-up images of two wetting paths under the same net stress (500 kPa), but starting from different initial moisture ratios for WR.

In order to propose an equation for $f(e_{wi})$, the reduction of e due to wetting from e_{wini} to e_{wi} under the net stress of p (Δe_i^p) was obtained using the experimental data and Eq. (8). Evidently, if $e_{wini} = e_{wd}$, then $\Delta e_i^p = \Delta e_{max}^p$.

$$\Delta e_i^p = e_i^p - e_{ini}^p \tag{8}$$

Using the obtained values of Δe_i^p, plots of e_w-Δe could be drawn. Fig. 11(a) shows schematic e_w-e (the continuous curve) and the corresponding e_w-Δe plots (the dashed curve) in which the initial condition was the driest point of interest (points A or A'). In this case, e_{wini} was equal to e_{wd}, hence, e_{ini}^p was equal to e_d^p. The equation that defined the dashed curve in Fig. 11(a) was, in fact, the $f(e_{wi})$ term in Eq. (7).

The dashed curve in Fig. 11(a) resembles the top half of a logistic function. A typical logistic function is shown in Fig. 11(b) with its top half presented in dashed line. The trend of the top half of this function shows that increasing the value of x initially causes a rapid increase in the value of f(x). However, the rate of increase leans towards zero after a specific value of x. This behavior could clearly be seen in Fig. 11(a) (the e_w-Δe curve) considering Δe as f(x) and e_w as x. A standard logistic function is presented in Eq. (9).

$$f(x) = \frac{L}{1 + \text{Exp}[-k(x - x_0)]} + C \tag{9}$$

where L is the curve's maximum value, x_0 is the x value of the curve's midpoint, k is a parameter that determines the steepness of the curve, Exp(x) is the exponential function, and C is a constant value.

In order to develop the logistic equation that fits the e_w-Δe curve presented in Fig. 11(a), standard logistic function's parameters were defined as the following:

- x: e_{wi}
- x_0: e_{wd}
- L: $2\Delta e_{max}^p$

The maximum achievable value was, in fact, Δe_{max}^p; however, since only half of the standard logistic function was used to fit the experimental data, Δe_{max}^p was multiplied by 2 to be taken as L. Accordingly, Eq. (9) could be converted into Eq. (10).

$$g(e_{wi}) = \frac{2\Delta e_{max}^p}{1 + \exp(-k(e_{wi} - e_{wd}))} + C \tag{10}$$

where $g(e_{wi})$ is a function that gives the reduction of void ratio due to wetting from e_{wd} to e_{wi} under the constant p.

Considering the fact that $g(e_{wi}) = 0$ where $e_{wi} = e_{wd}$, C equals Δe_{max}^p. Hence, Eq. (10) could be rewritten in the form of Eq. (11).

$$g(e_{wi}) = \Delta e_i^p = \Delta e_{max}^p \left(\frac{2}{1 + \exp(-k(e_{wi} - e_{wd}))} - 1 \right) \tag{11}$$

ARTICLE IN PRESS

E. Yaghoubi et al.   Soils and Foundations xxx (xxxx) xxx

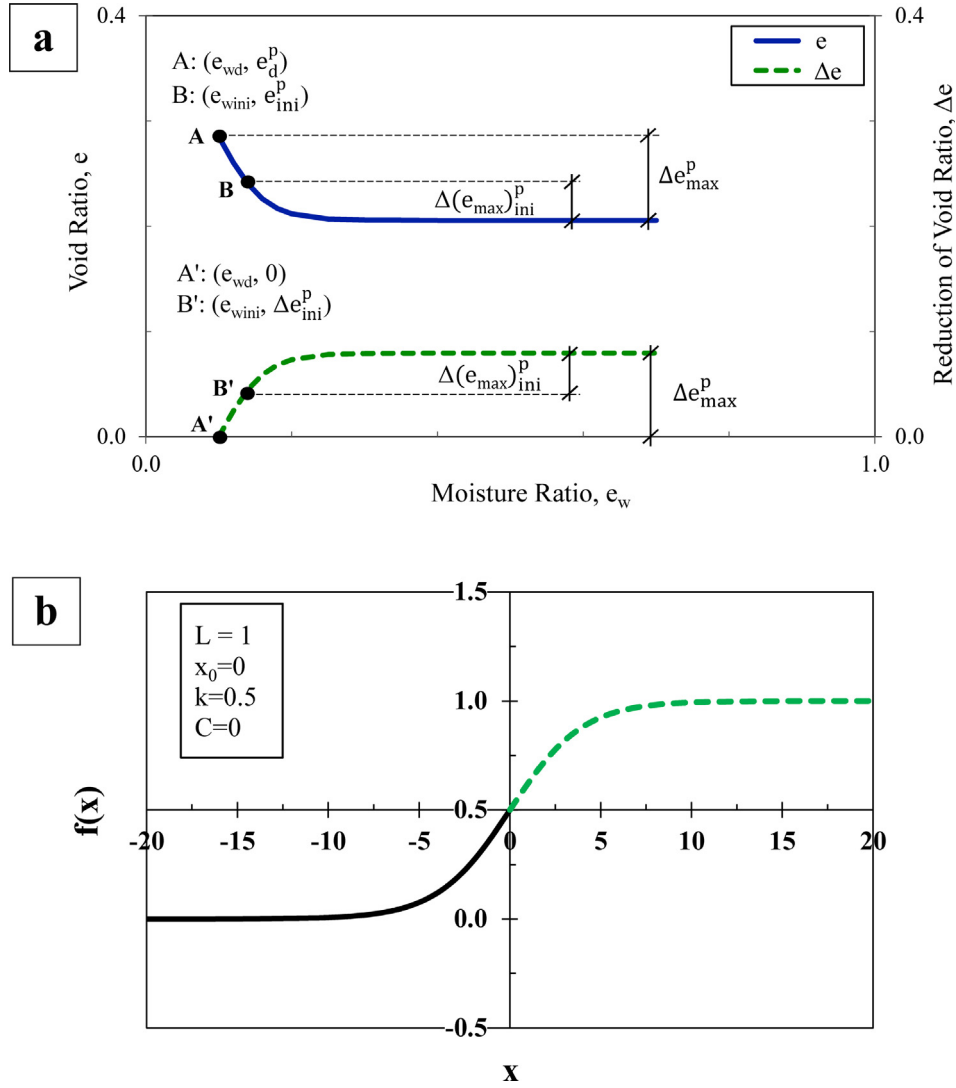Fig. 11. Defining the model parameters: (a) Schematic e_w-e and the corresponding e_w-Δe plots and (b) typical logistic function drawn using the presented parameters.

The value of Δe_{ini}^p could be obtained using Eq. (11) by taking e_{wini} as e_{wi}. Subsequently, $(\Delta e_{max})_{ini}^p$ was obtained using Eq. (12). For a clearer image, $(\Delta e_{max})_{ini}^p$ is shown in Fig. 11(a).

$$(\Delta e_{max})_{ini}^p = \Delta e_{max}^p - \Delta e_{ini}^p \tag{12}$$

Replacing Δe_{max}^p with $(\Delta e_{max})_{ini}^p$ and e_{wd} with e_{wini} in Eq. (11), $f(e_{wi})$ in Eq. (7) could be obtained using Eq. (13).

$$f(e_{wi}) = \Delta e_i^p$$

$$= (\Delta e_{max})_{ini}^p \left(\frac{2}{1 + \exp(-k(e_{wi} - e_{wini}))} - 1 \right) \tag{13}$$

Using Eqs. (1) and (13), the void ratio of the sample loaded to p and then wetted under the constant p was achievable, regardless of the initial e_w of the sample or the magnitude of the p under which wetting was carried out.

6. Verification of the proposed prediction model

In this section, the model proposed in Section 5 is evaluated by comparing the data measured through the laboratory experiments and the data predicted using the model.

6.1. Outline of the proposed procedure

The simplicity in obtaining the input parameters is the most important attribute of the proposed model. Table 9 presents a list of input parameters required for using the model and the tests or equations required for the determination of these parameters. Once the VCS is developed using Eq. (1) or experimental data, for any net stress of interest, the experimental data of only one LW path is required in order to predict any LW path starting from any e_{wini} between e_{wd} and saturation.

Table 9
Input parameters of the proposed model for LW state paths.

Input parameter	Required test/equation No.	Required No. of tests
e_{ini}^p	Eq. (1)	NA
Δe_{max}^p	LW path from driest condition to saturation condition under p	1 for each p of interest
$(\Delta e_{max})_{ini}^p$	Eq. (9)	NA
k	Fitting the data achieved from LW path (conducted for obtaining Δe_{max}^p) to Eq. (8)	NA

In order to use the model the procedure described below is proposed:

1) Determine e_{ini}^p before starting the wetting under constant p using Eq. (1).
2) Carry out a LW state path test from the driest point of interest (e_{wd}) to saturation condition (e_{ws}) under the p of interest to obtain e_d^p and e_s^p and the difference between these two values (Δe_{max}^p).
3) Obtain the value of k by fitting Eq. (11) to the data achieved from the LW state path carried out in Step 2.
4) Use Eq. (11) and input e_{wini} for e_{wi} to obtain Δe_{ini}^p.
5) Use Eq. (12) to obtain $(\Delta e_{max})_{ini}^p$.
6) Input $(\Delta e_{max})_{ini}^p$ in Eq. (13) to obtain $f(e_{wi})$ or Δe_i^p.
7) Input f(e_{wi}) in Eq. (7) to obtain e_i^p which is the void ratio of the sample, wetted from e_{wini} to e_{wi} of interest under constant p of interest.

The value of k depends on the type of material and the stress level in LW paths. The higher the volume change due to wetting and the lower the constant net stress during wetting, the greater the value of k would be. Values of k parameter achieved for LW paths for CB and WR subjected to different stress levels are presented in Table 10. The value of k for CB ranged between 5 and 10, whereas this range for WR extended between 12 and 17.8. Comparing the plots of LW state paths for WR and CB showed greater settlement (steeper curve in the e-e_w plane) for WR due to wetting; hence, higher k values. Interestingly, values of k and p showed a linear relationship for both CB and WR, with the reduction of k as the net stress increases for both CB and WR. The coefficient of determination (R^2) of 0.97 for CB and 0.99 for WR showed that k parameter could be estimated for any p between 100 kPa and 4000 kPa with a high accuracy. Thus, by obtaining k for the highest and lowest stress levels of interest, k parameters for any stress level in between can simply be interpolated.

Table 10
Values of k obtained in LW paths under different stress levels.

p (kPa)	CB	WR
100	10.0	17.8
500	9.2	17.3
1000	8.0	16.9
4000	5.0	12.0

6.2. Verification using independent loading-wetting paths

In this section, two LW paths for CB and two for WR were selected to be presented. The LW paths cover different stress levels and different initial moisture ratios. Fig. 12 shows the predicted and measured CB-L(100)W(sat)-2 and CB-L(4000)W(sat)-2 state paths in the e-e_w and e-log p planes. In the CB-L(100)W(sat)-2 (Fig. 12(a) and (b)), e_{wini} = 0.35, e_{ini}^p=0.720, $(\Delta e_{max})_{ini}^p$ = 0.023 and Δe_{max}^p = 0.063. For the net stress of 100 kPa, the value of k was 10. The predicted and measured paths were sufficiently close to each other verifying the model for predicting the LW state path under low net stress of 100 kPa.

In another attempt, a LW path obtained under the high net stress of 4000 kPa was selected to evaluate the model at high stress levels. Fig. 12(c) and (d) show the measured and predicted LW path for CB-L(4000)W(sat)-2. In this path, e_{wini} = 0.23, e_{ini}^p= 0.419, $(\Delta e_{max})_{ini}^p$ = 0.008, Δe_{max}^p= 0.009, and k = 5. Comparing the measured and predicted paths showed that the model was capable of predicting the LW state paths under high net stress of 4000 kPa. The low value of $(\Delta e_{max})_{ini}^p$ might seem negligible at the first glance. However, it is equivalent to the deformation of approximately 1.1 mm for a geotechnical layer with a thickness of 200 mm. In terms of pavements, the build-up of such a small deformation could result in significant deformations, such as rutting, in the long term.

Fig. 13(a) and (b) show the measured LW paths of WR-(100)W(sat)-2 and WR-L(1000)W(sat)-2 (Table 4) in comparison with those predicted by the model. The model parameters used for WR-(100)W(sat)-2 path included e_{wini} = 0.13, e_{ini}^p= 0.793, $(\Delta e_{max})_{ini}^p$ = 0.062, Δe_{max}^p=0.079, and k = 17.8. Once more, the predicted path closely followed the path obtained from the experiment. To evaluate the ability of the model under different stress levels, a higher net stress of 1000 kPa was also selected. Fig. 13(c) and (d) compare the predicted and experimentally obtained LW state path for WR under p = 1000 kPa, starting from e_{wini} = 0.14. Other model parameters included e_{ini}^p = 0.591, $(\Delta e_{max})_{ini}^p$ = 0.038, Δe_{max}^p=0.054, and k = 16.9. Alike the previous observations, the predicted LW path closely followed the measured path further verifying the capability of the proposed model in predicting the LW-induced deformations.

6.3. Verification using a combination of loading and wetting paths

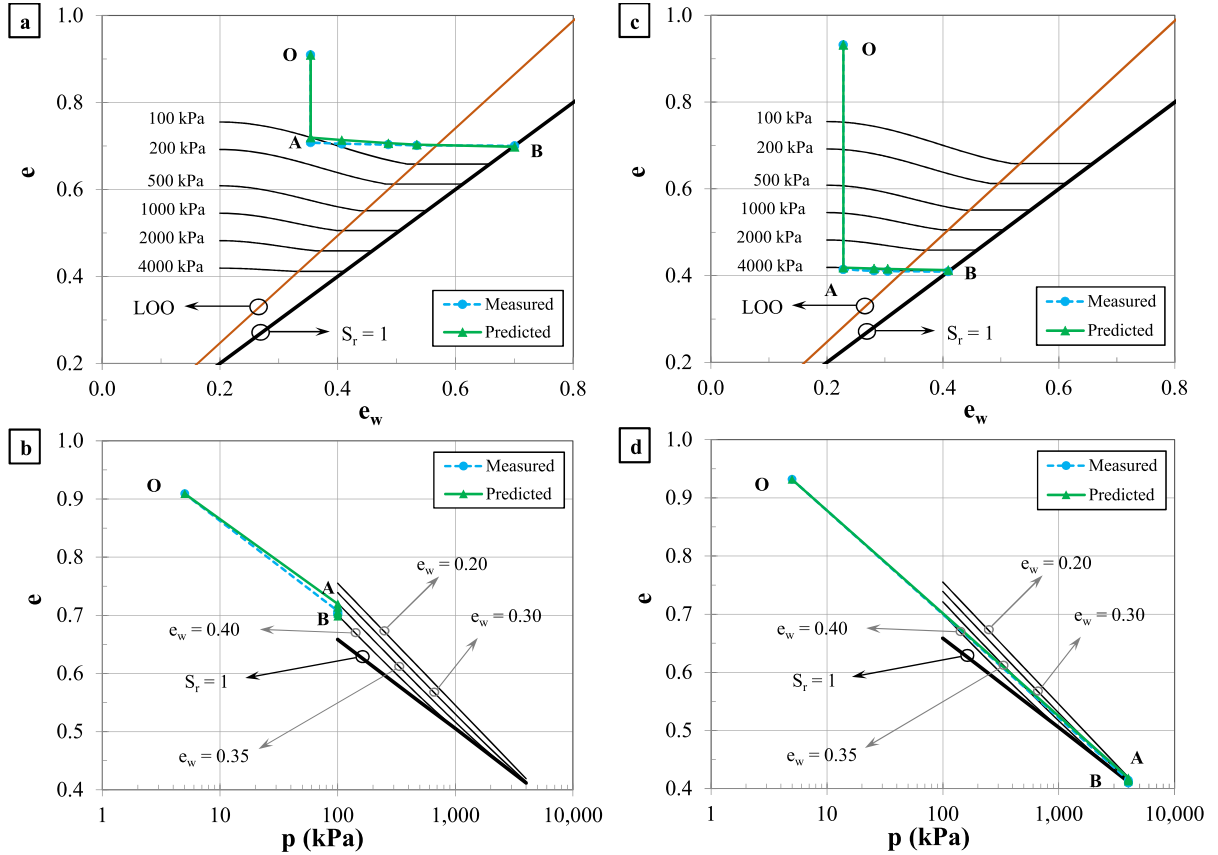In this section, two experimentally obtained combinations of loading and wetting paths (LWLW) starting from

Fig. 12. Predicted vs measured state paths of (a and b) CB-L(100)W(sat)-2 in e-e$_w$ plane and e-log p planes, respectively and (c and d) CB-L(4000)W(sat)-2 in e-e$_w$ plane and e-log p planes, respectively.

different initial conditions were selected to be presented and compared with their corresponding model-predicted paths in the e-e$_w$ and e-log p planes (Fig. 14).

In the first attempt the LWLW state path carried out on a CB sample loaded and wetted under two net stresses of 500 kPa and 1000 kPa was compared with the path predicted using the model (Fig. 14(a)). This was carried out through a double application of the model. In the first application, p = 500 kPa, e$_{wini}$ = 0.2, e_{ini}^p=0.609, $(\Delta e_{max})_{ini}^p$ =Δe_{max}^p = 0.028, and k = 10. The wetting path for this sample under the net stress of 500 kPa continued up to moisture ratio of 0.31. In the second application of the model, p = 1000 kPa, e$_{wini}$ = 0.31, e_{ini}^p=0.528, $(\Delta e_{max})_{ini}^p$ = 0.007, Δe_{max}^p = 0.012, and k = 9.2. Fig. 14(a) indicates that the predicted LWLW path closely follows the measured LWLW path verifying that the model was capable of predicting a combination of the loading and wetting paths.

In another attempt, the LWLW state path for a WR sample loaded to and wetted under two net stresses of 100 kPa and 500 kPa was predicted (Fig. 14(b)). Model parameters for the first LW path under p = 100 kPa included e$_{wini}$ = 0.12, e_{ini}^p= 0.793, $(\Delta e_{max})_{ini}^p$ = 0.66, Δe_{max}^p = 0.079, and k = 17.8. The sample was wetted under p = 100 kPa up to moisture ratio of 0.26 and the loading increased to the net stress of p = 500 kPa. In this part of the path, e$_{wini}$ = 0.26, e_{ini}^p=0.628, $(\Delta e_{max})_{ini}^p$ = 0.009,

Δe_{max}^p=0.081, and k = 17.3. Fig. 14(b) shows that the predicted and measured LWLW paths were very close.

In the BC paths of Fig. 14, the initial moisture condition of samples at the start of the second wetting paths was greater than the OMC of the material. In such moisture ratios, wetting path was more similar to a straight line rather than a curve. In spite of this, the model was developed such that this semi-linear trend was also well predicted which was an improvement compared to the previous model (Eq. (1)).

7. Discussion on the real-life application of the proposed model

The model developed in this research aims to provide a relationship between the moisture content, stress and the resultant deformation state in a granular geotechnical layer. External factors such as wetting through precipitation can cause further densification in compacted geostructures and hence, greater deformation than expected. The VCS and prediction model developed in this research aim to address two matters: a) to predict the ultimate deformation state (or density) of the granular material compacted using a known compaction effort at a determined moisture content and, and b) to predict the further deformation that
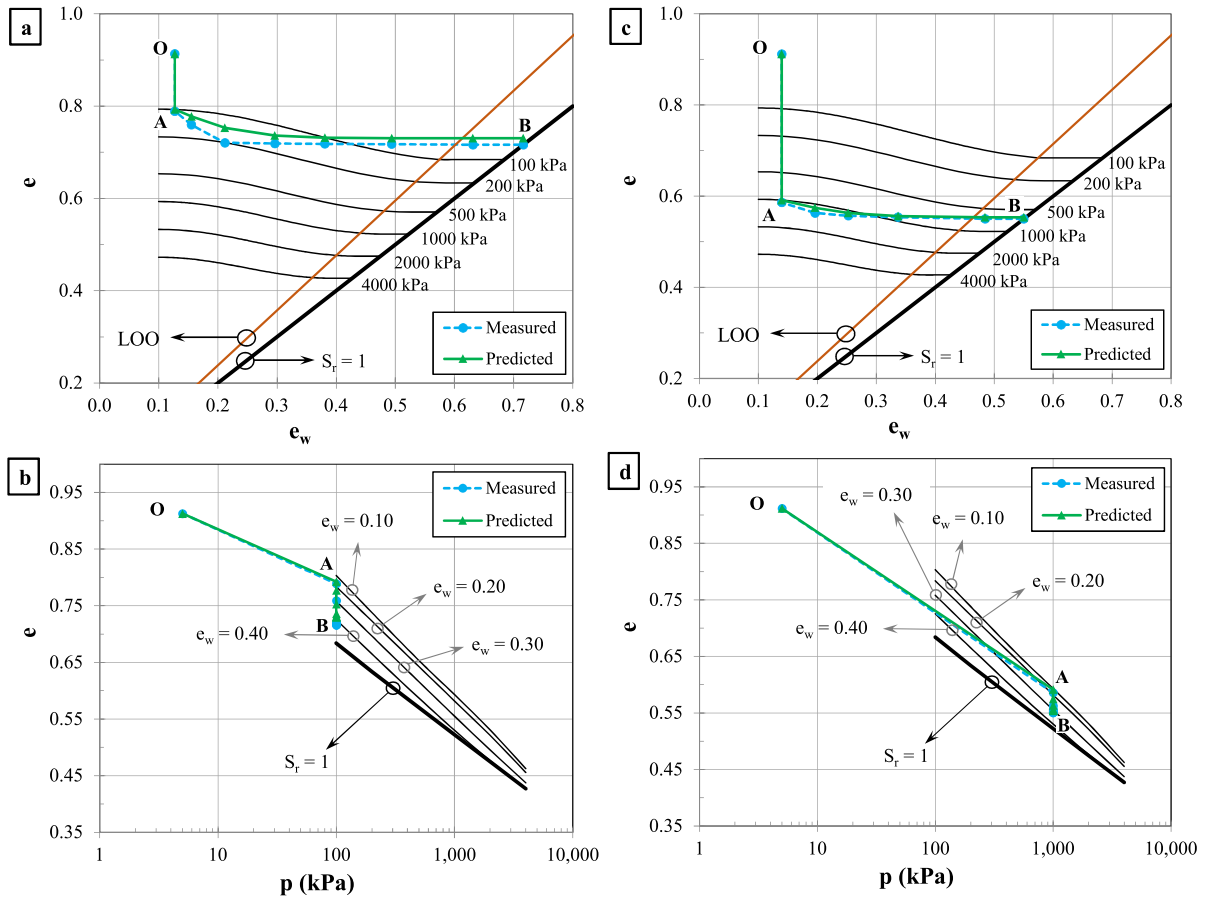
Fig. 13. Predicted vs measured state paths of (a and b) WR-(100)W(sat)-2 in e-e_w plane and e-log p planes, respectively and (c and d) WR-L(1000)W(sat)-2 in e-e_w plane and e-log p planes, respectively.
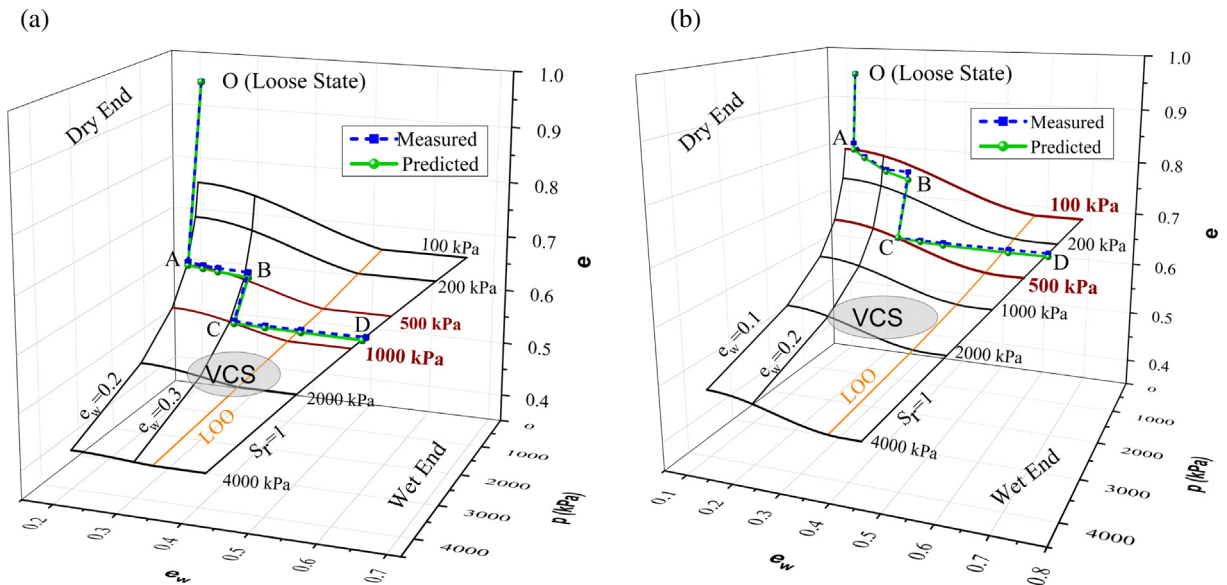

Fig. 14. Predicted vs measured state paths of (a) CB-L(500)W(0.31)L(1000)W(sat) and (b) WR-L(100)W(0.26)L(500)W(sat) in the space of e-e_w-p.

a compacted granular geostructure may exhibit due to a moisture content increase.

The LW state paths of this research were selected to simulate a geotechnical structure that is supporting a super-

structure and is currently subjected to wetting. A real-life example of such a state path is a granular foundation underneath the footing of a structure which is being wetted through precipitation or the leak in the water utilities of the

structure. In such a case, using Eq. (1), the initial deformation state of the compacted geostructure on the VCS can be determined. Next, by determining the input parameters presented in Table 9 through basic geotechnical tests, and following the steps outlined in Section 6.1, the final deformation state of the geostructure after wetting can be interpreted.

An instance of LUW state paths could be a lower layer of a road embankment compacted by a compaction roller, supported the weight of the embankment fill or pavement layers later placed on top of it and hence unloaded to a lower stress level compared to the compaction pressure, and is now being wetted as a result of flooding. Although, Eq. (1) can be utilized to predict the density of the geotechnical layer after being compacted at a determined moisture content, the VCS cannot fully interpret the state of the geostructure under unloading and wetting while being unloaded. In spiet of this, Eqs. (5) and (6) can be used to determine the hydric and the unloading coefficients in order to estimate the volume change due to unloading and wetting.

A real-life example of the LWLW path could be a granular foundation that was supporting the load of a footing and was next partially wetted through precipitation to a specific moisture content. Subsequently, the stress level on the foundation was increased by constructing a structure over the footing, and another precipitation occurred to increase the moisture content of the foundation. Once more, Eq. (1) and the procedure summarized in Section 6.1 can be used to predict the deformation state of the geostructure at any load or moisture conditions.

8. Conclusions

In this research, first, by extending the investigation on a previously developed virgin compaction surface (VCS) through several combinations of state paths the following conclusions were made:

- The developed VCS were unique in loading state paths;
- The uniqueness of the VCS with respect to wetting was only verified for the paths under constant net stresses including and greater than 2000 kPa.
- The Loading-Unloading-Wetting paths could partially be explained using the developed VCS. However, the surface could not predict the behavior of a complete path of LUW;
- The VCS were proved to be path-independent, at least with respect to incremental monotonic loading and wetting; and
- An application of the developed VCS could be the prediction of the density of the unbound granular geotechnical layer with a determined moisture content, compacted under different compaction energy and load levels.

Next, a moisture content-based volume change model was developed to predict the LW paths for the complete range of net stresses and moisture ratios used in the framework of this research. The model was verified for CB and WR in net stresses between 100 kPa and 4000 kPa with an initial moisture ratio within the driest condition and the wettest condition (saturation). In this research, the driest condition for CB (with e_w of 0.29 at its OMC) and WR (with e_w of 0.16 at its OMC) were respectively, 0.2 and 0.1. Model verification was done by comparing several LW paths predicted using the model with those obtained experimentally. The capability of the model in predicting a combination of LW paths was also shown in plots of measured-predicted LWLW state paths. These plots verified that the model is capable of predicting the volume change of the CB and WR samples regardless of the number of LW state path or the initial moisture condition. This excludes the wetting paths under a constant stress after unloading to a lower than the compaction (yield) stress in which the compacted sample is being wetted while being constantly loaded under a "lower than compaction" stress.

An example of the real-life application of this model could be the estimation of the settlement of a granular geotechnical layer due to changes in its moisture content during precipitation or flooding. This estimation would usually be very difficult to achieve due to the complication associated with conventional unsaturated volume change models. In the current model, however, using a straightforward procedure, the volumetric behavior of the unsaturated granular materials can be more simply interpreted and widely incorporated in the design and analysis of geotechnical structures.

It should be noted that the equations of the proposed model are obtained using the data from non-swelling materials that do not contain cementitious contents. Therefore, the model may not be applicable to the granular materials with the potential of swelling, such as clayey gravel and granular materials that contain cementitious particles in their matrix, such as recycled concrete aggregates.

The VCS and the prediction model are developed based on wetting paths, while unbound geostructures can be subject to both wetting and drying. Compacted granular materials are not expected to show volume change as a result of drying, and hence, the current research has focused on the wetting paths. Nevertheless, potential future research is proposed to investigate the behavior of the granular materials in drying paths as well as wetting. Also, the experiments in this research were carried out under static loading. Potential research proposed for the future can hence be the investigation of the volumetric behavior of compacted unsaturated granular materials under cyclic loading, vibration and/or creep loading conditions.

References

Abeyrathne, A., 2017. A new modelling approach for compacted clayey soils using specific water volume as a state variable. Monash University. PhD.

Al-Taie, A., Disfani, M., Evans, R., Arulrajah, A., 2019. Collapse and swell of lime stabilized expansive clays in void ratio-moisture ratio–net stress space. Int. J. Geomech. 19 (9), 04019105.

Al-Taie, A., Disfani, M., Evans, R., Arulrajah, A., Horpibulsuk, S., 2018. Volumetric behavior and soil water characteristic curve of untreated and lime-stabilized reactive clay. Int. J. Geomech. 19 (2), 04018192.

Alonso, E.E., Gens, A., Josa, A., 1990. A constitutive model for partially saturated soils. Geotechnique 40 (3), 405–430.

Aubertin, M., Mbonimpa, M., Bussière, B., Chapuis, R.P., 2003. A model to predict the water retention curve from basic geotechnical properties. Can. Geotech. J. 40 (6), 1104–1122.

Azam, A., Cameron, D., Gabr, A., Rahman, M., 2014. Matric Suction in Recycled Unbound Granular Materials. Geo-Congress 2014: Geo-characterization and Modeling for Sustainability.

Azam, A., Cameron, D., Rahman, M., 2013. Model for prediction of resilient modulus incorporating matric suction for recycled unbound granular materials. Can. Geotech. J. 50 (11), 1143–1158.

Ba, M., Nokkaew, K., Fall, M., Tinjum, J.M., 2013. Effect of matric suction on resilient modulus of compacted aggregate base courses. Geotech. Geol. Eng. 31 (5), 1497–1510.

Cary, C.E., Zapata, C.E., 2011. Resilient modulus for unsaturated unbound materials. Road Mater. Pavement Des. 12 (3), 615–638.

Cui, Y., Delage, P., 1996. Yielding and plastic behaviour of an unsaturated compacted silt. Geotechnique 46 (2), 291–311.

Fleureau, J.M., Verbrugge, J.C., Huergo, P.J., Gomes Correia, A., Kheirbek-Saoud, S., 2002. Aspects of the behaviour of compacted clayey soils on drying and wetting paths. Can. Geotech. J. 39 (6), 1341–1357.

Foster, C., Ahlvin, R., 1954. Stresses and deflections induced by a uniform circular load. Highway Research Board Proceedings.

Fredlund, D.G., Rahardjo, H., 1993. Soil Mechanics for Unsaturated Soils. John Wiley & Sons.

Gould, S.J.F., Kodikara, J., Rajeev, P., Zhao, X.L., Burn, S., 2011. A void ratio - water content - net stress model for environmentally stabilized expansive soils. Can. Geotech. J. 48 (6), 867–877.

Heath, A.C., Pestana, J.M., Harvey, J.T., Bejerano, M.O., 2004. Normalizing behavior of unsaturated granular pavement materials. J. Geotech. Geoenviron. Eng. 130 (9), 896–904.

Houlsby, G., 1997. The work input to an unsaturated granular material. Geotechnique 47 (1), 193–196.

Islam, T., 2015. A study of volumetric behaviour of compacted clayey soils in the void ratio, moisture ratio and net stress space, Monash University. Faculty of Engineering. Department of Civil Engineering.

Islam, T., Kodikara, J., 2015. Interpretation of the loading–wetting behaviour of compacted soils within the "MPK" framework. Part I: Static compaction 1. Can. Geotech. J. 53 (5), 783–805.

Jayasundara, C., Kodikara, J., Zhou, A., 2019. A volumetric yield surface for compacted soils based on constant water content testing. E3S Web of Conferences. EDP Sci.

Kieu, M., Mahler, A., 2018. A study on the relationship between matric suction and the void ratio and moisture content of a compacted unsaturated soil. Periodica Polytech. Civil Eng. 62 (3), 709–716.

Kodikara, J., 2012. New framework for volumetric constitutive behaviour of compacted unsaturated soils. Can. Geotech. J. 49 (11), 1227–1243.

Lu, N., 2008. Is matric suction a stress variable? J. Geotech. Geoenviron. Eng. 134 (7), 899–905.

Lu, N., Likos, W.J., 2004. Unsaturated Soil Mechanics. Hoboken, New Jersey, Wiley.

Macari-Pasqualino, E.J., Runesson, K., Sture, S., 1994. Response prediction of granular materials at low effective stresses. J. Geotech. Eng. 120 (7), 1252–1268.

Matyas, E.L., Radhakrishna, H., 1968. Volume change characteristics of partially saturated soils. Geotechnique 18 (4), 432–448.

Perera, Y., Zapata, C., Houston, W., Houston, S., 2005. Prediction of the soil water characteristic curve based on grain-size-distribution and index properties. In: Rathje, E.M. (Ed.), Advances in Pavement Engineering. Geotechnical Special Publication 130, pp. 49–60.

Pham, H.Q., Fredlund, D.G., 2011. Volume–mass unsaturated soil constitutive model for drying–wetting under isotropic loading–unloading conditions. Can. Geotech. J. 48 (2), 280–313.

Raveendiraraj, A., 2009. Coupling of Mechanical Behaviour and Water Retention Behaviour in Unsaturated Soils. University of Glasgow.

Sun, D.A., Sheng, D., Xu, Y., 2007. Collapse behaviour of unsaturated compacted soil with different initial densities. Can. Geotech. J. 44(6), 673–686.

Vassallo, R., Mancuso, C., Vinale, F., 2007. Effects of net stress and suction history on the small strain stiffness of a compacted clayey silt. Can. Geotech. J. 44 (4), 447–462.

Wheeler, S., Sharma, R., Buisson, M., 2003. Coupling of hydraulic hysteresis and stress–strain behaviour in unsaturated soils. Geotechnique 53 (1), 41–54.

Witczak, M., Kaloush, K., Pellinen, T., El-Basyouny, M., Von Quintus, H., 2002. NCHRP Report 465: Simple Performance Test for Superpave Mix Design, TRB, National Research Council, Washington, D.C.

Yaghoubi, E., Disfani, M.M., Arulrajah, A., Kodikara, J., 2016. Impact of compaction methods on resilient response of unsaturated granular pavement material. Proc. Eng. 143, 323–330.

Yaghoubi, E., Disfani, M.M., Arulrajah, A., Kodikara, J., 2017. Impact of compaction method on mechanical characteristics of unbound granular recycled materials. Road Mater. Pavement Des., 1–23

Yaghoubi, E., Disfani, M.M., Arulrajah, A., Kodikara, J., 2019. Development of a void ratio-moisture ratio-net stress framework for the prediction of the volumetric behavior of unsaturated granular materials. Soils Found. 59 (2), 443–457.

Zhang, X., Li, L., 2011. Limitations in the constitutive modeling of unsaturated soils and solutions. Int. J. Geomech. 11 (3), 174–185.

Zhang, X., Lytton, R.L., 2009. Modified state-surface approach to the study of unsaturated soil behavior. Part I: Basic concept. Can. Geotech. J. 46 (5), 536–552.

Zhang, X., Lytton, R.L., 2012. Modified state-surface approach to the study of unsaturated soil behavior. Part III: Modeling of coupled hydromechanical effect. Can. Geotech. J. 49 (1), 98–120.